Engineering NiO/PEDOT: PSS Hybrid Electrode for Enhanced Charge-Storage Kinetics, Energy Density, and Long-Term Cycling Stability

Syed Shehzad Hassan[1], Muhammad Imran[2], Asaad Alluhaybi[3], Muhammad Imran Bashir[4], Muhammad Javed Akhtar[1], Muhammad Ahmad Rohaan[5]
[1]Institute of Physics (IOP), Government College (GC) Lahore
[2]Department of Electronics, Government College (GC) Lahore
[3]Department of Physical Sciences, College of science, University of Jeddah, Jeddah, 23890, Saudi Arabia
[4]University of Lahore (UOL)
[5]LACAS, Burki
*Correspondence: imranawan@gcu.edu.pk, syedshehzadhassan95@gmail.com, aalluhaybi@uj.edu.sa, imranbashirmphil@gmail.com, mj28304@gmail.com, ahmadrohaan4343@gmail.com

Citation | Hassan. S. S, Imran. M, Alluhaybi. A, Bashir. M. I, Akhtar. M. J, Rohaan. M. A, "Engineering NiO/PEDOT: PSS Hybrid Electrode for Enhanced Charge-Storage Kinetics, Energy Density, and Long-Term Cycling Stability", IJIST, Vol. 8 Issue. 10 pp 4122-4144, November 2026

Received | Oct 26, 2026 **Revised |** Nov 08, 2026 **Accepted |** Nov 11, 2026 **Published |** Nov 13, 2026.

The development of efficient electrode materials with excellent redox reversibility and long-term cycling stability remains a major research challenge in electrochemical energy storage. In this study, for the first time, a conducting polymer-assisted NiO composite was developed by incorporating poly(3,4-ethylenedioxythiophene) (styrenesulfonate) (PEDOT) into hydrothermally synthesized NiO nanoparticles through a facile physical mixing approach. 1.5 mL PEDOT was used with nickel oxide (NiO) to evaluate the influence on the electrochemical behavior of NiO-based electrodes. The integrity of the crystalline NiO structure and the effective inclusion of the conducting polymer were verified by structural and morphological analyses performed using X-ray diffraction (XRD), scanning electron microscopy (SEM), and Fourier-transform infrared spectroscopy (FTIR). A three-electrode setup with a multichannel workstation with a 3 M KOH electrolyte was used for the electrochemical experiments. The specific capacitance of the NiO-PEDOT composite was recorded as 413 F g^{-1}, which is higher than that of pristine NiO (243 F g^{-1}) at 1 A g^{-1}. In addition, the oxidation b-value increased from 0.51 to 0.78 according to kinetic analysis, suggesting that surface-controlled charge-storage processes and redox chemistry played a more prominent role. In comparison to pure NiO, which loses 8.9% of its initial capacitance after 5000 redox cycles, the composite shows outstanding cycling stability, maintaining 98.7% after 5000 cycles. Moreover, compared to pure NiO, representing the densities of 4.134 Wh kg^{-1} and 212 W kg^{-1} and coulomb efficiency of 89%, respectively, the NiO-PEDOT electrode showed densities of 14.34 Wh kg^{-1} and 511 W kg^{-1} and coulomb efficiency of 93%. The conductive polymer network promoted interparticle connections, resulting in improved electron transport, and preserving electrochemical activity throughout the cycling stability evaluation. This study establishes the foundation for integrating PEDOT into NiO-based materials to augment structural constancy, redox reversibility, and efficiency, paving a new research corridor for PEDOT integration into metal oxides.

Keywords: Nickel Oxide, PEDOT, Conducting Polymer, Supercapacitors, Pseudocapacitance, Energy Storage, Cycling Stability

Introduction:

Supercapacitors serve as essential energy storage components for flexible electronic devices, electric cars, and grid-scale energy management systems[1]. The attributes of supercapacitors include elevated power density, fast charge-discharge dynamics, and prolonged cycling longevity. To attain competitive energy densities, it is crucial to employ electrode materials that include abundant redox-active sites, effective routes for electron and ion transport, and robust structural stability across repeated charge and discharge cycles [2]. Transition metal oxides are thoroughly explored as electrode materials because of their proficiency in energy storage and conversio. Nickel oxide (NiO) is distinguished by its theoretical promise in energy storage and conversio functions[3]. The abundance of the material, eco-friendly characteristics, and significant capacity linked to the Ni^{2+}/Ni^{3+} redox pair make it a promising solution for the rising energy requirements. Nonetheless, the pragmatic obstacles associated with metal oxides, such as inadequate conductivity, charge clustering, structural instability, and restricted access to active areas, hinder the full exploitation of NiO as an electrochemically active electrode material [4].

These issues are evident in almost all transition-metal oxides and their composites. Accordingly, [5] used a solution combustion method to make spinel-type high-entropy oxide $(MnFeCoNiZn)_3O_4$ nanoparticles and studied their electrical properties. The electrode had a specific capacitance of 288.7 F/g at 3 A/g. The sample lost 50% of specific capacitance after 5,000 charge–discharge cycles. The asymmetric supercapacitor showed power density of 746 W/kg and an energy density of 7.9 Wh/kg. In the same way, [6] reported binder-free NiO thin-film electrodes for flexible hybrid asymmetric solid-state supercapacitors using the successive ionic layer adsorption and reaction (SILAR) method. The device achieved a specific capacitance of 165 F/g, an energy density of 58.87 Wh/kg, and a power density of 347 W/kg, with 79% cycle stability after 5,000 cycles. In another study, [7] developed the hierarchical $Mn_2O_3@MnO_2$ core–shell nanofibers reporting a specific capacitance of 225 F/g and 86.5% capacitance retention after 5,000 cycles, highlighting the influence of core–shell architecture on electrochemical stability. Furthermore, [8] reviewed transition-metal molybdates and their graphene-based composites, emphasizing the influence of composition, morphology, and synthesis conditions on their electrochemical properties and energy-storage performance. More recently, [9] synthesized $NiCo_2O_4$ and $NiCo_2O_4$/rGO composite electrodes and investigated their charge-storage properties. The $NiCo_2O_4$/rGO electrode attained a specific capacitance of 998 F/g in a three-electrode setup, while the related asymmetric device demonstrated a specific capacitance of 93.7 F/g, an energy density of 29.2 Wh/kg, and a power density of 750 W/kg, maintaining 85% capacitance retention after 5,000 cycles. [10] has highlighted an additional, still largely unaddressed failure mode: leaching of metal-oxide species during electrochemical operation, driven by concurrent oxygen-evolution (OER) and hydrogen-evolution (HER) side reactions. This dissolution not only depletes active material but also compromises electrode–electrolyte interfaces, thereby accelerating capacity fade. These studies demonstrate that improving specific capacitance while maintaining structural integrity and long-term cycling stability remains an unresolved riddle in transition-metal oxide-based supercapacitors. The incorporation of conductive carbon-based polymers with metal oxides offers a promising strategy to mitigate metal leaching by enhancing interfacial interactions and improving structural stability. The optimum incorporation of multi-walled carbon nanotubes into metal oxide nanocomposites can significantly enhance electronic conductivity, electrolyte accessibility and cycling stability, underscoring the synergistic benefit of conductive scaffolding [11].

Among all carbon based materials, PEDOT is a promising conductive polymer candidate for metal oxide-based supercapacitor electrodes due to its ability to suppress particle

agglomeration by providing a uniform conductive matrix [12]. Furthermore, its polymeric network can enhance interfacial interactions, help retain metal oxide particles within the composite structure, and mitigate metal leaching during repeated electrochemical cycling. Its high electrical conductivity can also facilitate charge transport and improve the electrochemical stability of the composite electrode.

Therefore, further investigation of metal-oxide composites with PEDOT:PSS is necessary to explore their potential for improved electrochemical performance and cycling stability. Critically, a conformal PEDOT:PSS coating can encapsulate metal-oxide nanoparticles, sterically hinder agglomeration, buffer local volume expansion, and physically isolate the oxide surface from aggressive electrolyte environments that promote dissolution [13][14][15]. Despite these advantages, systematic optimization of PEDOT:PSS loading in NiO-based supercapacitor electrodes has not been reported. Prior studies have examined PEDOT or PEDOT:PSS in combination with nickel hydroxide or mixed nickel-containing oxides, but the binary NiO/PEDOT:PSS system remains unexplored with respect to the precise polymer-to-oxide ratio that balances electronic connectivity against ion-access restrictions.

In the present work, NiO/PEDOT:PSS composite electrodes were fabricated using the aqueous PEDOT:PSS dispersion (1.5 mL). 1.5 ml of PEDOT:PSS was used because of the previously reported optimum response for metal oxides/sulfides [16][17]. These compositions were chosen to map the trade-off between polymer-mediated inter-particle bridging—which is expected to improve electronic percolation and mechanical cohesion—and potential blockage of redox-active NiO surfaces by excess polymer. The central hypothesis is about the intermediate polymer content will simultaneously (i) establish continuous conductive pathways, (ii) encapsulate NiO particles sufficiently to suppress agglomeration and leaching, and (iii) preserve electrolyte accessibility to the oxide surface. Insufficient polymer is predicted to leave discontinuous electrical contacts, whereas excess polymer is expected to impede ion transport and diminish the Faradaic contribution of NiO.

Till today, this work constitutes the first investigation of binary NiO/PEDOT:PSS electrodes across a defined range of polymer loadings for supercapacitor applications. By correlating polymer content with interfacial connectivity, electrolyte accessibility, resistance to metal-oxide leaching, and electrochemical stability, the study establishes a rational design framework that can be extended to other metal-oxide/PEDOT:PSS systems.

Experimental Section:

Chemicals:

Nickel nitrate hexahydrate ($Ni(NO_3)_2 \cdot 6H_2O$) served as the starting material for producing NiO, while PEDOT was introduced to the oxide matrix to fabricate the NiO–PEDOT composite. Urea was added to facilitate precipitation during synthesis. Acetone, ethanol (C_2H_5OH), and double-deionized water were used as processing and cleaning media. N-methyl-2-pyrrolidone (NMP) was selected as the solvent for dissolving the PVDF binder, whereas carbon black was incorporated to improve electrode conductivity. Before electrode preparation, the substrate was cleaned thoroughly with acetone and double-deionized water. The aqueous 3 M KOH electrolyte was used to evaluate the electrochemical performance.

Synthesis of NiO:

NiO nanoparticles were prepared through a hydrothermal synthesis route following the procedure described in [18], with minor methodological details specified herein. $Ni(NO_3)_2 \cdot 6H_2O$ and urea served as the nickel source and precipitating agent, respectively. Both precursors were dissolved in 40 mL of deionized (DI) water using a nickel nitrate-to-urea molar ratio of 1:2. The sample was stirred continuously for 30 min and then transferred into a Teflon-lined stainless-steel autoclave and kept at 130 °C for 4 h. Following the hydrothermal reaction, the autoclave was naturally cooled to room temperature. The

precipitates were washed three times with DI water and ethanol, followed by centrifugation and drying at 80 °C for 48 h. The material was annealed at 400 °C for 2 h.

Synthesis of NiO-PEDOT:PSS:

NiO-PEDOT:PSS composites were prepared through a physical mixing approach using different volumes of PEDOT:PSS. Three composite samples were prepared by incorporating 0.5, 1.0, and 1.5 mL of PEDOT:PSS into 3 mg of synthesized NiO nanoparticles. Each mixture was spread in DI water and imperiled to vigorous stirring for 5 hours to ensure uniform mixing and dispersion of the constituent materials. Following the mixing process, the resulting suspensions were dried for 24 hours to obtain the NiO-PEDOT:PSS composite materials with different PEDOT:PSS contents.

Characterization Techniques:

Physical Characterizations:

X-ray Diffraction Spectroscopy (XRD):

The X-ray diffraction (XRD) patterns for pure NiO and the NiO–PEDOT:PSS composite are presented in Figure 1(a,b). Both samples exhibit distinct and well-defined diffraction peaks that correspond to the face-centered cubic (fcc) structure of NiO (space group $Fm\bar{3}mFm$), consistent with standard JCPDS card No. 47-1049 as shown in Figure 1(c). The characteristic reflections associated with the (111), (200), (220), (311), and (222) planes are observed at nearly identical 2θ positions in both patterns, indicating the preserved crystalline phase of NiO after the incorporation of PEDOT:PSS.

A slight increase in the full width at half maximum (FWHM) is noted for the NiO–PEDOT:PSS composite compared to pure NiO. This modest peak broadening is attributed to the presence of the PEDOT:PSS matrix, which introduces limited local strain and partially restricts crystallite growth during composite formation. Importantly, the overall crystallinity of NiO is not disturbed by the polymer; the peaks remain intense and sharp, indicating the long-range ordered structure of the oxide is preserved.

The Scherrer equation was used to get the average crystallite size [19]:

$$D=\frac{K\lambda}{\beta \cos \Theta}(1)$$

where K is the shape factor (0.9), λ is the X-ray wavelength (Cu Kα, 0.15406 nm), β is the FWHM in radians, and θ is the Bragg angle. Using the most intense (200) reflection, the crystallite size of pure NiO was found to be approximately 28–32 nm, while that of the NiO–PEDOT:PSS composite was slightly smaller (approximately 24–27 nm). This reduction is dependable upon the observed increase in FWHM and supports the role of PEDOT:PSS in moderating crystallite growth without compromising the crystalline integrity of NiO.

The absence of any sharp peaks or significant peak shifts further confirms PEDOT:PSS exists in an amorphous state and does not form a secondary crystalline phase or induce lattice distortion in the NiO structure. Collectively, these results demonstrate the polymer successfully encapsulates the NiO nanoparticles while maintaining the structural purity and crystallinity of the oxide phase.

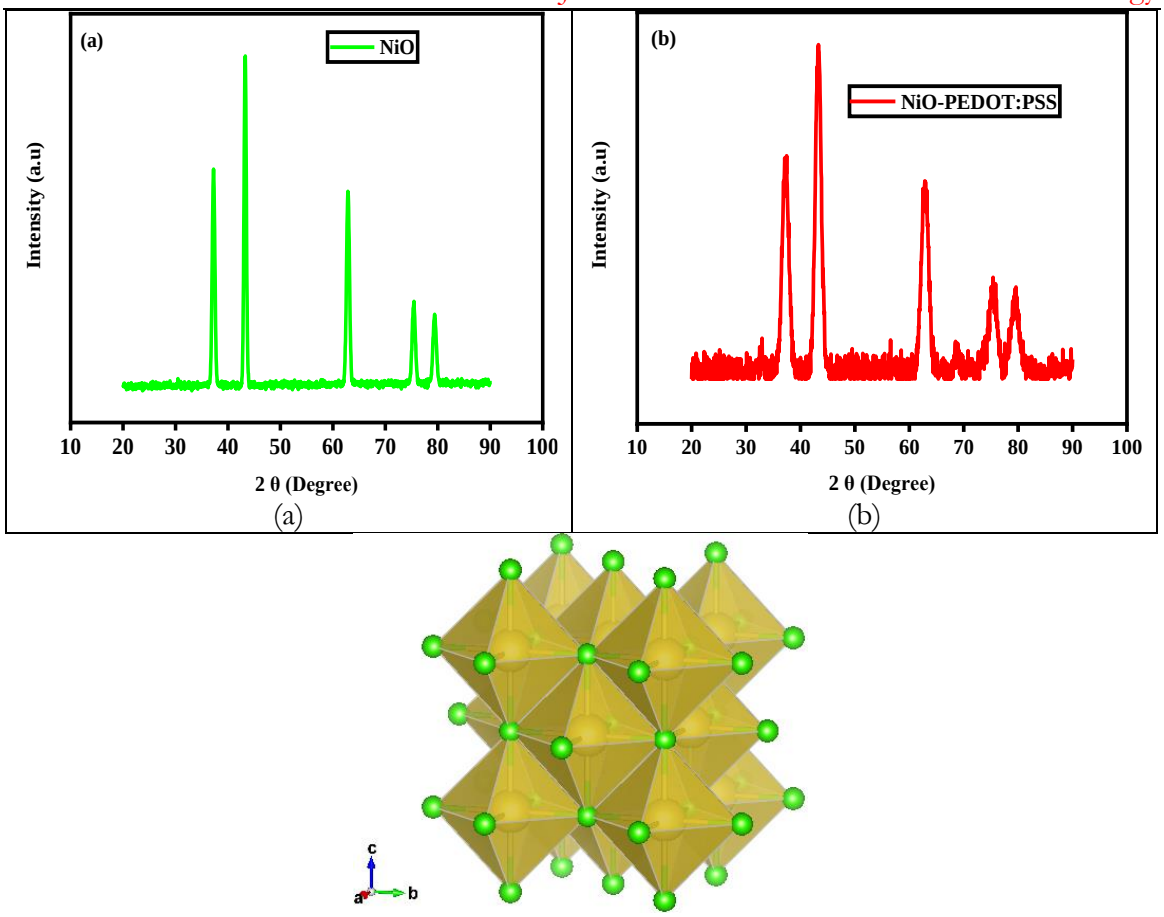


Figure 1. (a) XRD of nickel oxide (NiO), (b) XRD of nickel oxide-PEDOT:PSS (NiO-PEDOT:PSS), (c) VESTA generated face-centered cubic (fcc) structure of NiO (space group $Fm\bar{3}mFm$)

SEM Analysis:

The surface morphology of pristine NiO and the NiO–PEDOT:PSS composite was examined by scanning electron microscopy (SEM), as shown in Figures 2(a) and 2(b).

The pristine NiO (left panel, 5 000× magnification) exhibits an irregular plate-like and flake-like morphology. The particles appear as discrete, angular platelets with relatively sharp edges and a broad size distribution, typically ranging from several hundred nanometers to a few micrometers as shown in Figure 2(a). Significant agglomeration is evident, with many flakes stacked together. This tendency toward aggregation is characteristic of pure metal-oxide nanoparticles and can limit electrolyte accessibility during electrochemical operation [20].

In contrast, the NiO–PEDOT:PSS composite (right panel, 5000× magnification) in Figure 2(b) exhibits a notably altered morphology. The plate-like NiO particles demonstrate a uniform dispersion and appear to be partially coated or interconnected by a thin, continuous polymeric layer, as shown in Figure 2(c) at a resolution of 7500. The sharp edges of the pristine flakes are softened, resulting in smoother and more rounded overall particle surfaces. The polymer matrix effectively reduces inter-particle agglomeration, creating a more open and interconnected architecture with improved spatial distribution of the oxide particles. This encapsulation by PEDOT:PSS helps maintain interparticle contacts while generating additional interstitial voids that facilitate electrolyte penetration [21].

The morphological evolution confirms the PEDOT:PSS successfully coats and bridges the NiO platelets without completely obscuring their surfaces. Such a hybrid microstructure is expected to enhance electronic connectivity between NiO particles, suppress

excessive agglomeration, and develop interconnecting networks that are highly desirable for supercapacitor electrode applications.

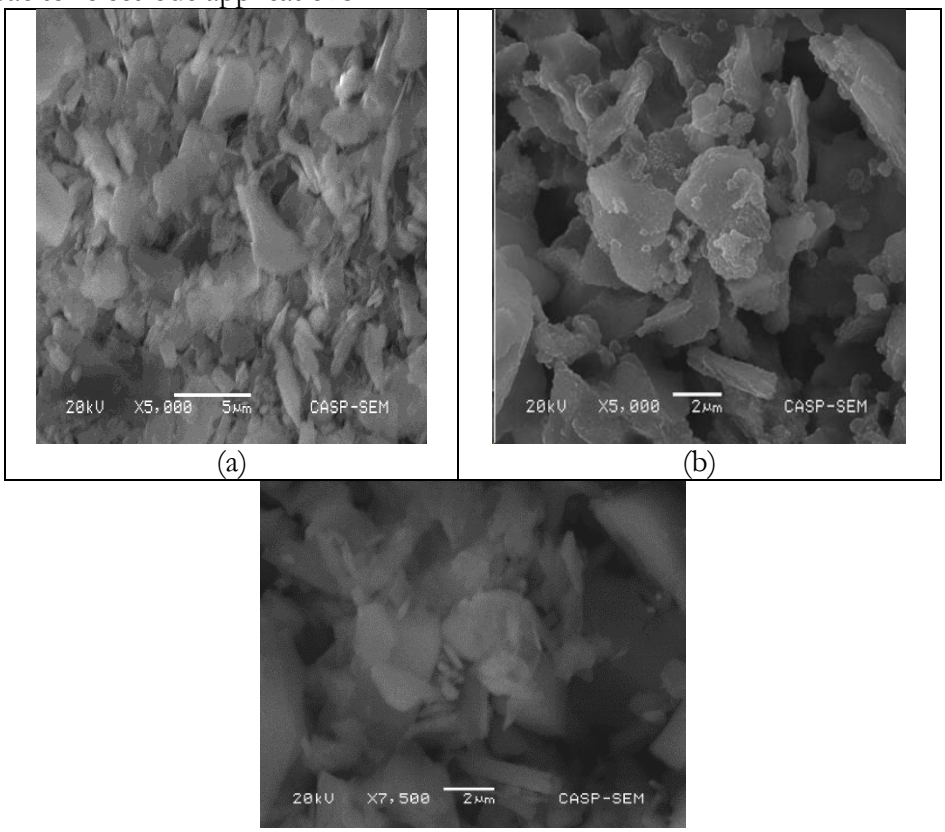


Figure 2. (a) SEM structure of NiO, (b,c) SEM structure of NiO-PEDOT:PSS at (5000 and 7500) resolution

FTIR Analysis:

The Fourier-transform infrared (FTIR) spectra of pristine NiO and the NiO–PEDOT:PSS composite are presented in Figure 3.

Both samples exhibit a strong, broad absorption band in the low-wavenumber region (approximately 400–600 cm^{-1}), which is characteristic of the Ni–O stretching vibration and confirms the presence of the nickel oxide lattice [22]. Additional weaker bands observed in the mid-infrared region of pure NiO can be attributed to surface hydroxyl groups and adsorbed water molecules (typically O–H bending and stretching modes) [23].

In the NiO–PEDOT:PSS composite spectrum (red), several intensified features appear that are significantly weaker in pure NiO. The most notable difference is highlighted in the region marked by the purple circle, where a distinct absorption emerges. This feature is assigned to vibrational modes associated with the PEDOT:PSS polymer, specifically the C–S stretching and C–O–C stretching vibrations of the ethylenedioxy group in the PEDOT chain, as well as the sulfonate (S–O) related modes of the PSS component [22][24][25][26]. Additional subtle bands in the 800–1600 cm^{-1} range further support the successful incorporation of the conducting polymer [27].

The overall spectral profile indicates the fundamental Ni–O framework remains intact after composite formation, while the appearance of polymer-specific absorptions confirms the presence of PEDOT:PSS on the surface of the NiO particles. The slight attenuation and broadening of certain NiO-related bands are consistent with partial surface coverage by the polymer matrix. Collectively, the FTIR results provide clear evidence of the successful formation of the NiO–PEDOT:PSS hybrid without disruption of the oxide chemical structure.

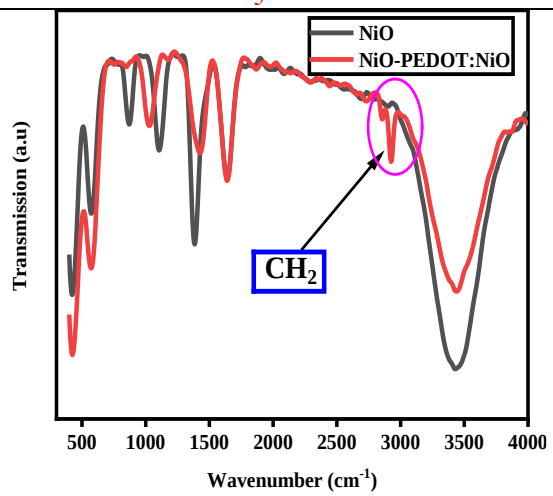


Figure 3. FTIR Spectrum of NiO and NiO-PEDOT:PSS

Electrochemical Analysis:

Electrode Preparation:

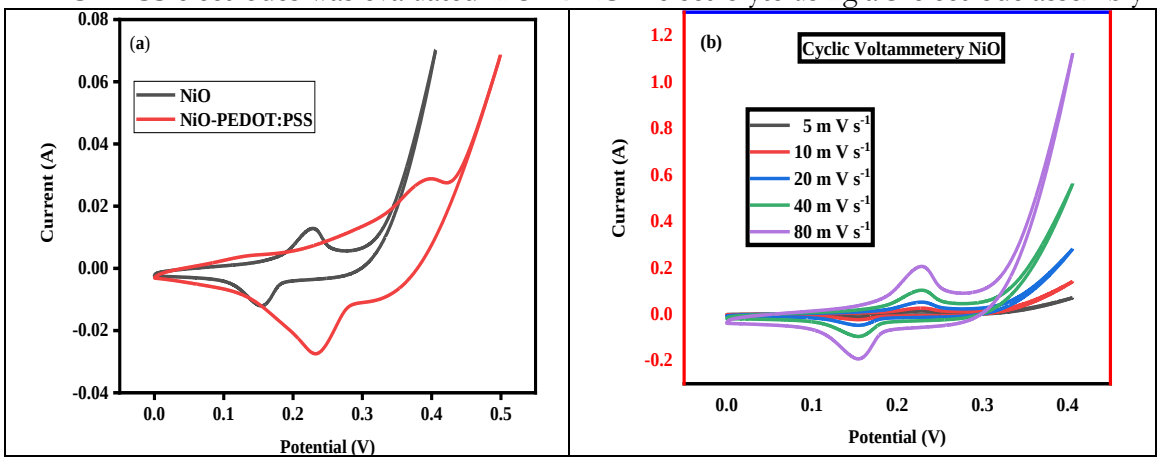
The dried NiO and NiO-PEDOT:PSS composites, were prepared by physically mixing carbon black, polyvinylidene fluoride (PVDF) and active materials in a mass ratio of 8:1:1 in N-methyl-2-pyrrolidone (NMP), as a solvent. To obtain a homogeneous slurry with suitable consistency for electrode coating, the active materials were mixed thoroughly. Meanwhile, the nickel foam was cleaned using 33% HCl and acetone. The prepared slurry was uniformly coated onto the nickel foam of the area of approximately 1 cm^2. Subsequently, the coated electrodes were dried at 60 °C for 12 hours to remove the residual solvent and obtain stable electrode coatings. The active material loading was maintained at 3 mg cm^{-2}. Energy and power density were calculated by following equations [28]:

$$E = \frac{Cs\ V^2}{2 \times 3.6} \quad (2)$$

$$P = \frac{E \times 3600}{\Delta t} \quad (3)$$

Electrochemical Analysis in Three-Electrode System:

The cyclic voltammetry (CV) measurements were performed at different scan rates from (5-80 m V s^{-1}) to investigate the electrochemical behavior and charge-storage characteristics of the prepared electrodes as shown in the Figure 4 (a,b). The galvanostatic charge–discharge (GCD) measurements were conducted at current densities ranging from 1 to 5 A g^{-1} in the Figure 5 (a,b). The electrochemical response of the NiO and NiO-PEDOT:PSS electrodes was evaluated in 3 M KOH electrolyte using a 3-electrode assembly.



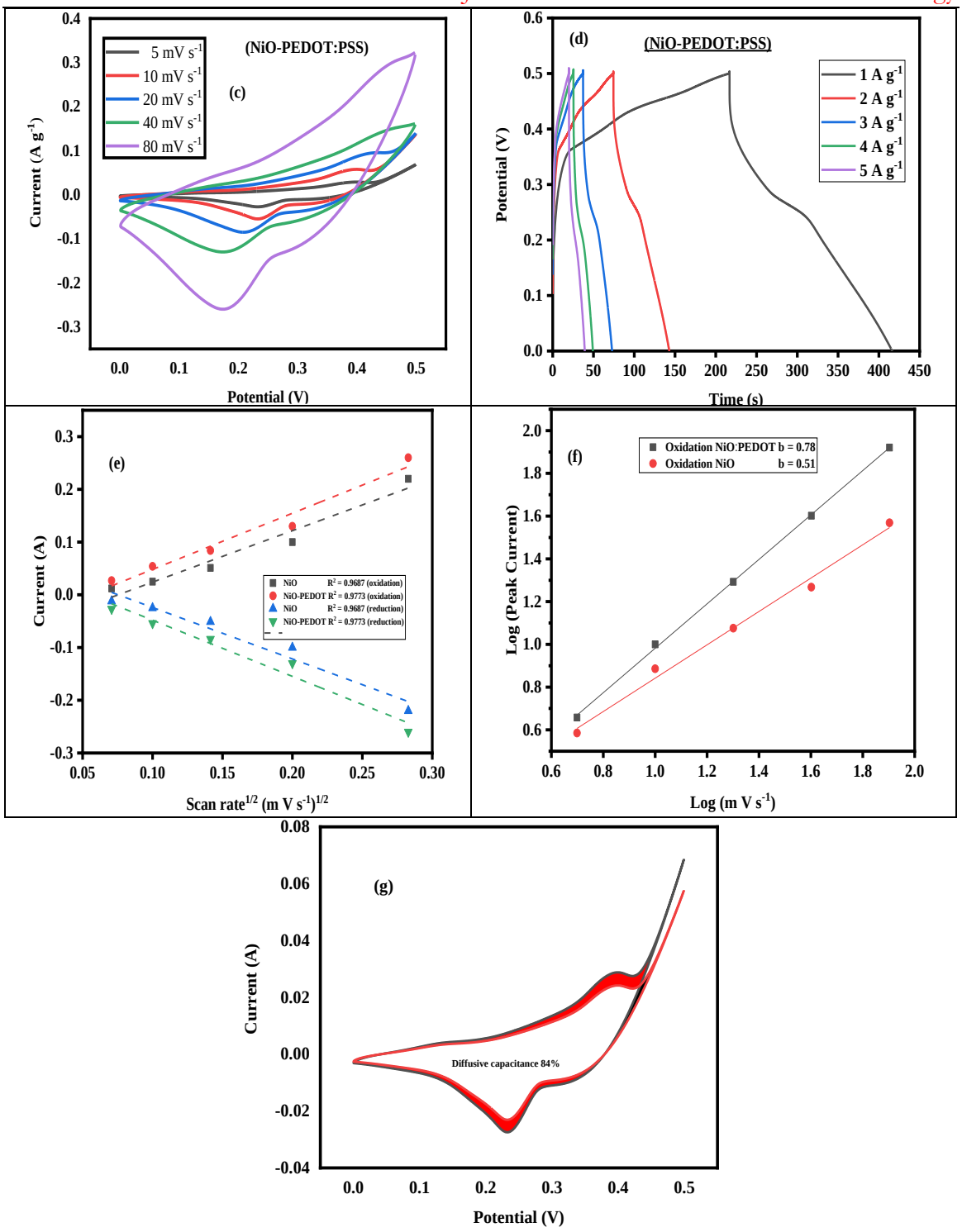


Figure 4. Cyclic voltammetry analysis of NiO and NiO-PEDOT:PSS electrodes in 3 M KOH electrolyte: (a) Comparative CV profiles of NiO and NiO-PEDOT:PSS electrodes; (b,c) CV profiles at different scan rates ranging from 5 to 80 mV s^{-1}; (d) gcd analysis of NiO-PEDOT:PSS electrode from 1 A g^{-1} to 5 A g^{-1}(e) power-law analysis illustrating the relationship between square root scan rate Vs Ip, (f) logarithmic peak current and logarithmic scan rate for determination of b-values; (g) diffusive and capacitive contribution at 5 m V s^{-1}

The CV profiles of both electrodes exhibit distinct redox features, indicating the presence of Faradaic charge-storage processes associated with pseudocapacitive behavior. These redox

characteristics can be attributed primarily to the reversible conversion between nickel-based oxidation states in the alkaline electrolyte [29].

Figure 5(a,b) presents a comparison of the GCD profiles of the NiO and NiO-PEDOT:PSS electrodes. The nonlinear charge–discharge profiles and the presence of voltage plateaus are consistent with the Faradaic characteristics observed in the CV measurements. The specific capacitance was calculated using the following equation [30]:

$$Csp=\frac{I\Delta t}{m\,\Delta V}(4)$$

where (I) represents the discharge current, Δ t is the discharge time, m is the mass of the active material, and ΔV represents the effective potential window during discharge.

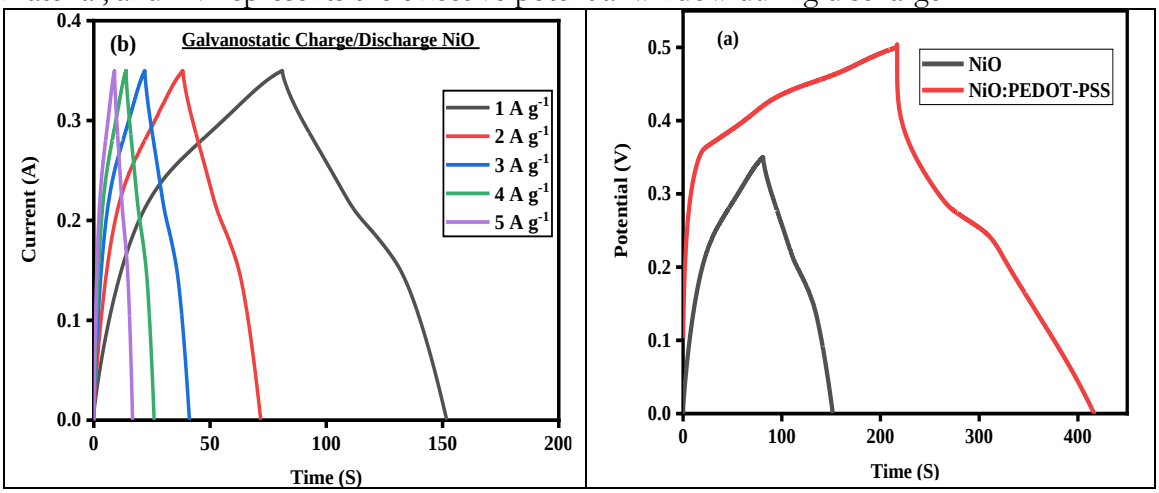


Figure 5. Galvanostatic charge–discharge (GCD) analysis of NiO and NiO-PEDOT:PSS electrodes in 3 M KOH electrolyte: (a) Comparative GCD profiles at 1 A g^{-1}; (b) GCD profiles of NiO electrodes at different current densities ranging from 1 to 5 A g^{-1};

The possible electrochemical reaction responsible for charge storage in NiO can be expressed as follows [30]:

$$NiO+OH\ NiOOH+e^{-1}$$

The incorporation of PEDOT:PSS, a conductive polymer network, into the NiO matrix can facilitate electron transport and improve the electrochemical accessibility of active sites [31]. Also the conductive nature of PEDOT:PSS may reduce the internal resistance of the composite electrode and facilitate charge transfer during electrochemical cycling [32]. Additionally, the polymer component may provide extra charge-storage sites via reversible redox processes. The integration of nickel oxide and conductive polymer enhances the electrochemical performance of the composite electrode. Figure 4(a) presents the comparative cyclic voltammetry profiles of pristine NiO and NiO-PEDOT:PSS electrodes. The composite electrode demonstrates a larger enclosed CV area, indicating increased electrochemical activity and enhanced charge-storage capacity. Resultantly PEDOT:PSS enhances the accessibility of electroactive NiO sites by augmenting electronic connectivity within the electrode structure.

Figures 4(b,c) demonstrate the CV responses of the prepared electrodes at different scan rates ranging from 5 to 80 mV s^{-1}. The persistence of the characteristic CV profiles with increasing scan rate indicates the optimum electrode response for the Faradaic charge-storage characteristics under different electrochemical operating conditions. The changes in redox peak positions with increasing scan rate are associated with the polarization and kinetic limitations of the electrochemical reactions [33]. Figure 4(d) represents the GCD response of NiO-PEDOT:PSS. The shift in the active redox region from 0.05–0.35 V to 0.1–0.5 V may be attributed to the incorporation of the PEDOT:PSS scaffold into the NiO matrix resulted in enhanced chemistry of electrode[34].

To investigate the charge-storage kinetics, the relationship between the peak current (i) and scan rate (v) was examined using the power-law equation[35]:

$$i=av^b \quad (5)$$

Taking the logarithm of both sides gives:

$$\log(i)=\log(a)+b\log(v) \quad (6)$$

where a and b represent adjustable parameters, and the b-value is determined from the slope of the linear relationship between log(i) and log(v). A b-value approaching 0.5 indicates predominantly diffusion-controlled charge storage, whereas a value approaching 1.0 suggests a predominantly surface-controlled capacitive process [36]. The plotted power-law in Figure 4 (f) analysis indicates an oxidation b-value of approximately 0.51 for pristine NiO, which suggests a substantial diffusion-controlled contribution. In comparison, the NiO-PEDOT:PSS composite exhibits a higher oxidation b-value of approximately 0.78, indicating an increased contribution from surface-controlled charge-storage processes resulted in enhanced potential window [37]. This improvement can be associated with the conductive polymer network, which may facilitate electron transport and improve the accessibility of electroactive sites during rapid electrochemical reactions [38].

The distinction between capacitive and diffusion-controlled charge-storage contributions can further be investigated using Dunn's method [39]:

$$i(V)=k_1 v+k_2 v^{1/2} \quad (7)$$

where (k_1v) represents the surface-controlled capacitive contribution and $k_2v^{1/2}$ represents the diffusion-controlled contribution. The corresponding parameters can be determined by plotting $i(V)/v^{1/2}$ vs $v^{1/2}$ at selected potentials. This analysis provides quantitative information about the contribution of each charge-storage mechanism at different scan rates.

Figures 4(e) illustrate the square root of scan rate Vs peak current responses of pristine NiO and NiO-PEDOT:PSS electrodes. The NiO-PEDOT:PSS composite demonstrates considerably higher specific capacitance than pristine NiO across the investigated current densities. At 1 A g^{-1}, the composite electrode delivers a specific capacitance of 413 F g^{-1}, whereas pristine NiO exhibits 243 F g^{-1}. Similarly, at current densities of 2, 3, 4, and 5 A g^{-1}, the NiO-PEDOT:PSS electrode exhibits specific capacitances of 272, 210, 192, and 181 F g^{-1}, respectively. In comparison, the corresponding values for pristine NiO are 193, 162, 137, and 109 F g^{-1}, respectively.

The coulomb efficiency of both of the electrodes is calculated by the following equation:

$$\% \eta = \frac{t_d}{t_c} \times 100 \quad (8)$$

The NiO-PEDOT:PSS electrode shows a coulombic efficiency of 93% remarkably greater than pristine NiO 89%. The superior coulomb efficiency is due to the enhanced electro-ionic conductivity due to conductive carbon po;ymer PEDOT:PSS. The superior electrochemical response of NiO-PEDOT:PSS composite can also be attributed to the complementary electrochemical characteristics of the metal oxide and conductive polymer. NiO offers Faradaic redox-active locations for charge retention, whereas PEDOT:PSS enhances electronic conductivity and promotes charge transfer over the composite electrode. Moreover, the polymer matrix could enhance the dispersion and availability of electroactive NiO particles [40], thereby facilitating a more effective use of the active substance [41]. The synergistic effects improve the electrochemical efficacy of the composite electrode.

The specific capacitance diminishes as current density rises for both electrodes, a common trait seen in pseudocapacitive materials. At high current densities, the reduced discharge duration may limit the complete exploitation of electroactive sites, particularly those located in the electrode's interior regions. Nonetheless, the NiO-PEDOT:PSS composite

demonstrates superior specific capacitance relative to pure NiO over the tested current-density spectrum, signifying improved charge-storage efficiency and rate performance.

EIS Spectroscopy:

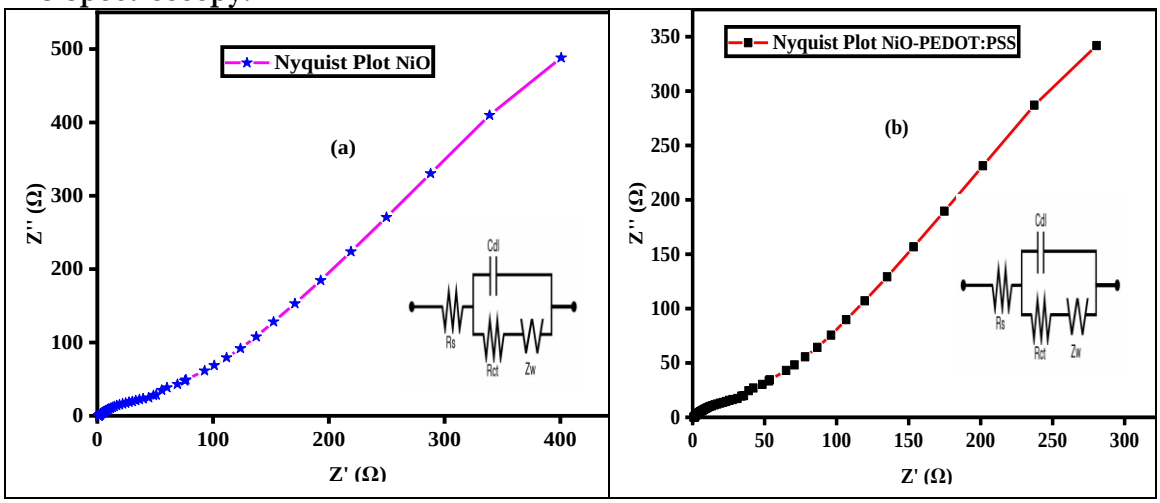


Figure 6. Electrochemical impedance spectroscopy (EIS) analysis of the prepared electrodes: (a) Nyquist plot of pristine NiO electrode; (b) Nyquist plot of NiO-PEDOT:PSS composite electrode. The insets represent the proposed equivalent electrical circuit comprising solution resistance (Rs), double-layer capacitance (Cdl), charge-transfer resistance (Rct), and Warburg impedance (Zw).

Electrochemical impedance spectroscopy (EIS) was employed to investigate the interfacial charge-transfer characteristics, ionic diffusion behavior, and electrical resistance of the pristine NiO and NiO-PEDOT:PSS electrodes. The Nyquist plots provide information about the electrode–electrolyte interface and the electrochemical processes occurring during charge storage. The equivalent circuits for both samples are shown in Figure 6(a,b).

The Nyquist response of both electrodes exhibits a predominantly inclined, non-semicircular profile, suggesting the contribution of capacitive and diffusion-related processes at the electrode–electrolyte interface [42]. The inclined low-frequency response is associated with ion diffusion within the electrode structure and electrolyte penetration into the electroactive material. Equivalent electrical circuit is presented in the inset which consists of solution resistance (Rs), double-layer capacitance (Cdl), charge-transfer resistance (Rct), and Warburg impedance (Zw). The solution resistance denotes the inherent resistance of the electrolyte in conjunction with other ohmic elements inside the electrochemical system [43]. Rs is charge-transfer resistance measuring the resistance associated with Faradaic processes at the electrode-electrolyte boundary. Conversely, the Warburg element delineates the resistance linked to the diffusion of electrolyte ions. The NiO-PEDOT:PSS composite is expected to exhibit improved interfacial charge-transfer characteristics owing to the incorporation of the conductive PEDOT:PSS polymer [44]. The polymer can establish additional electronic conduction pathways between NiO particles, potentially facilitating electron transport and improving the utilization of electroactive sites [45]. Furthermore, the interaction between the conducting polymer and NiO may improve the electrode's overall electrical connectivity and contribute to its enhanced electrochemical response. These characteristics are consistent with the higher specific capacitance obtained for the NiO-PEDOT:PSS electrode during galvanostatic charge–discharge measurements. Overall, EIS provides complementary information regarding the interfacial and diffusion-related behavior of the prepared electrodes. The equivalent-circuit parameters were extracted using nonlinear least-squares fitting in Python with SciPy is reported (Supporting file S1) in table 2 as given below in Table 1:

Table 1. EIS equivalent circuit fitted parameters from Python with SciPhy

Parameter	Fitted value		Unit
	NiO-PEDOT:PSS	NiO	
Rs	0.89	1.2181	Ω
Rct	5.44	11.4800	Ω
CPE-T (Q)	0.0977	0.001738	$S \cdot s^n$
CPE-P (n)	1.224	0.9559	Dimensionless
Warburg coefficient (σ)	73.997	103.9903	$\Omega \cdot s^{-1/2}$
Inductance (L)	931 x 10^{-5}	1431 × 10^{-6}	H

The incorporation of NiO-PEDOT:PSS offers a promising approach by improving the overall electrochemical kinetics as given in Tble 2. The improved charge-transfer properties of the NiO-PEDOT:PSS electrodes contribute to enhanced charge-storage performance of hybrid NiO-PEDOT:PSS.

Cyclic Stability:

The long-term cycling stability of pristine NiO and NiO-PEDOT:PSS electrodes was investigated to evaluate their capacitance retention and electrochemical durability during repeated charge–discharge cycles. As illustrated in Figure 7 (a,b), both electrodes exhibit a gradual decrease in specific capacitance with increasing cycle number. However, a significant difference in capacitance retention is observed between the two electrodes.

The pristine NiO electrode preserves over 89% of its original specific capacitance following the cycling test, signifying a capacitance reduction of roughly 11%. The reduction in specific capacitance may result from the leaching process and by-product OER reactions attributed to the elevated oxidation state of NiO [46]. In contrast, the NiO-PEDOT:PSS composite has markedly improved cycle stability, retaining 98.7% of its original specific capacitance under the same cycling conditions. This signifies a capacitance reduction of only 1.3%, highlighting the beneficial function of PEDOT:PSS in improving the electrochemical longevity of the composite electrode.

The enhanced cycling stability of NiO-PEDOT:PSS is attributed to the incorporation of the conductive polymer, which improves electrical connectivity among NiO particles and facilitates charge transfer over successive electrochemical cycles. Furthermore, the PEDOT:PSS network may assist in preserving structural integrity and minimizing the degradation of electrical contact between electroactive particles throughout repeated charge–discharge cycles [47]. These effects can boost the utilization of electroactive sites.

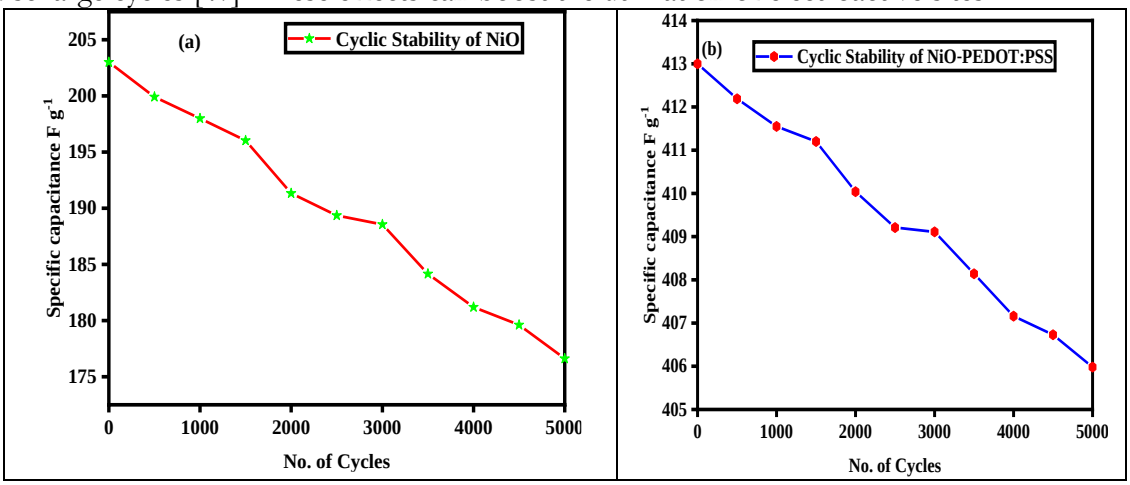


Figure 7. Cycling stability of (a) pristine NiO and (b) NiO-PEDOT:PSS electrodes, demonstrating capacitance retention of 89% and 98.7%, respectively, after repeated charge–discharge cycling.

The retention of 98.7% of the initial capacitance of PEDOT:PSS based NiO supports the potential of the composite as an electrode material for electrochemical energy-storage applications.

Furthermore the NiO-PEDOT:PSS shown energy density of 14.34 Wh kg^{-1} and power density of 511 W kg^{-1} greater than pristine NiO of 4.134 Wh kg^{-1} and 212 W kg^{-1}.

Table 2. Comparison Table of previously reported work

Sr. No.	Metal oxide / composite	Synthesis method	Electrolyte	Ref.	Specific capacitance (F/g)
1	NiO	Chemical bath deposition	1 M KOH	[48]	309
2	NiO hollow spheres	Chemical bath deposition	2 M KOH	[49]	346
3	NiO nanofibers modified with citric acid	Electrospinning	6 M KOH*	[50]	336
4	NiO nanotubes	Template-assisted chemical deposition and annealing	6 M KOH	[51]	266
5	NiO/graphene	Hydrothermal		[52]	384
6	N-doped graphene/NiO	Two-step synthesis		[53]	342
7	NiO/activated carbon (50:50)	Co-precipitation followed by physical blending	6 M KOH (electrode); 1 M $TEABF_4$/PC (device)	[54]	325
8	NiO/activated carbon	Hydrothermal in-situ synthesis followed by high-temperature activation		[55]	226.5

The comparative electrochemical results reported in Table 2 establish that incorporating PEDOT:PSS into NiO provides a beneficial approach for improving the electrochemical characteristics of nickel oxide electrodes. The improved electronic transport, enhanced accessibility of electroactive sites, and additional charge-storage contributions associated with the conducting polymer collectively explain the superior performance of the NiO-PEDOT:PSS composite.

Conclusion:

To address the weak electrical conductivity and cycling stability of pristine NiO electrodes, a conducting polymer-assisted NiO (NiO-PEDOT) composite was synthesized via a facile physical mixing method. The PEDOT polymer created a conducting polymer matrix surrounding the NiO particles, leading to enhanced NiO particle dispersion and interconnection while retaining the characteristic crystalline structure of NiO. The XRD data revealed that the composite maintained the face-centered cubic phase of NiO, whereas the FTIR data confirmed the existence of the distinctive functional groups of PEDOT. In addition, a change in surface morphology by SEM showed reduced aggregation of particles with a good distribution of the oxide particles. Electrochemical measurements revealed a significant enhancement in charge storage performance upon addition of PEDOT. The specific capacitance of the NiO–PEDOT composite was 413 F g^{-1} at 1 A g^{-1}, compared with 243 F g^{-1} at 1 A g^{-1} for pristine NiO. The kinetic study confirmed the enhanced electrochemical behavior of the composite, where the oxidation b-value increased from 0.51

for pure NiO to 0.78 for the composite, indicating the participation of surface-controlled charge-storage mechanisms. In addition, the composite showed better electrochemical performance than pristine NiO over the range of current densities tested (1-5 A g^{-1}), which indicates good rate capability. More impressively, it had better long-term cycle stability and outstanding coulomb efficiency of 93%. The NiO-PEDOT electrode maintained 98.7% of the capacitance after 5000 charge-discharge cycles (vs. ~89% for pure NiO). This improvement demonstrates the beneficial effect of the conducting polymer on the electrical contact and electrochemical activity of the electrode during cycling. Additionally, the composite has a specific energy density of 14.34 Wh kg^{-1} (3.5 times that of NiO which is 4.134 Wh kg^{-1}) and a specific power density of 511 W kg^{-1} (which is 2.4 times that of NiO which is 212 W kg^{-1}). These results show that the electrochemical properties and stability of electrodes based on NiO can be improved by simply introducing PEDOT.

Future Research Perspectives and Innovation:

Future research should focus on optimizing the PEDOT-to-NiO ratio and investigating interfacial mechanisms using advanced characterization techniques to further improve electrochemical stability. The development of ternary NiO–PEDOT–carbon nanocomposites and metal oxide heterostructures may enhance conductivity, charge transfer, and structural durability. Furthermore, long-term cycling studies and practical two-electrode configurations are recommended to assess their potential for high-performance and scalable energy-storage applications.

References:

[1] A. G. Olabi, Q. Abbas, A. Al Makky, and M. A. Abdelkareem, "Supercapacitors as next generation energy storage devices: Properties and applications," *Energy*, vol. 248, p. 123617, Jun. 2022, doi: 10.1016/J.ENERGY.2022.123617.

[2] F. Wang *et al.*, "Latest advances in supercapacitors: from new electrode materials to novel device designs," *Chem. Soc. Rev.*, vol. 46, no. 22, pp. 6816–6854, Nov. 2017, doi: 10.1039/C7CS00205J.

[3] S. S. Hassan *et al.*, "Tailoring NiO nanostructures via solvent engineering: structural, optical and supercapacitor performance insights," *Ionics 2026 325*, vol. 32, no. 5, pp. 5709–5724, Apr. 2026, doi: 10.1007/S11581-026-07109-7.

[4] M. Ben Arbia and E. Comini, "Growth Processing and Strategies: A Way to Improve the Gas Sensing Performance of Nickel Oxide-Based Devices," *Chemosens. 2024, Vol. 12, Page 45*, vol. 12, no. 3, p. 45, Mar. 2024, doi: 10.3390/CHEMOSENSORS12030045.

[5] R, Arun S; Jacob, George, "Exploring the charge storage ability of the spinel-type high entropy oxide (MnFeCoNiZn)3O4 nanoparticles for supercapacitor applications," *CEJA*, 2025, [Online]. Available: https://ui.adsabs.harvard.edu/abs/2025CEJA...2100708R/abstract

[6] M. B. Kumbhar, V. V. Patil, V. S. Chandak, J. L. Gunjakar, and P. M. Kulal, "Enhancing energy storage with binder-free nickel oxide cathodes in flexible hybrid asymmetric solid-state supercapacitors," *J. Alloys Compd.*, vol. 1010, p. 177311, Jan. 2025, doi: 10.1016/J.JALLCOM.2024.177311.

[7] W. Lu, Y. Li, M. Yang, X. Jiang, Y. Zhang, and Y. Xing, "Construction of Hierarchical Mn2O3@MnO2Core-Shell Nanofibers for Enhanced Performance Supercapacitor Electrodes," *ACS Appl. Energy Mater.*, vol. 3, no. 9, pp. 8190–8197, Sep. 2020, doi: 10.1021/ACSAEM.0C00392.

[8] D. S. Sawant, S. B. Kulkarni, D. P. Dubal, and G. M. Lohar, "Transition Metal Molybdates Emerging Materials for High-Performance Supercapacitors: A Machine Learning Analysis," *Batter. Energy*, vol. 4, no. 3, May 2025, doi:

10.1002/BTE2.20240073.

[9] R. Govindaraju, A. Balakrishnan, N. M. Chidambaram, V. Thirumal, P. Rajkumar, and J. Kim, "Integrated Effects of NiCo2O4 and Reduced Graphene Oxide in High-Performance Supercapacitor Systems," *Inorganics*, vol. 14, no. 2, p. 33, Feb. 2026, doi: 10.3390/INORGANICS14020033/S1.

[10] S. S. Hassan *et al.*, "Synergistic biphasic Cr_2O_3–ZrO_2/MWCNT nanocomposite: exceptional electrochemical performance for next-generation supercapacitors," *Ionics 2026*, pp. 1–23, Oct. 2026, doi: 10.1007/S11581-026-07594-W.

[11] K. Hyun, J. H. Lee, and S. J. Kim, "Incorporation Of Multi-Walled Carbon Nanotubes Into Oxide Layer Formed On Al Alloy By Plasma Electrolytic Oxidation," *Surf. Rev. Lett.*, vol. 27, no. 11, pp. 1–7, Nov. 2020, doi: 10.1142/S0218625X20500079.

[12] S. A. Thomas, J. Cherusseri, and D. N. Rajendran, "Hierarchical Two-Dimensional Layered Nickel Disulfide (NiS2)@PEDOT:PSS Nanocomposites as Battery-Type Electrodes for Battery-Type Supercapacitors with High Energy Density," *Electrochem 2024, Vol. 5, Pages 298-313*, vol. 5, no. 3, pp. 298–313, Jul. 2024, doi: 10.3390/ELECTROCHEM5030019.

[13] Ö. Yağci, M. B. Arvas, and S. Yazar, "Facile and single step produced Ba:Sn-codoped PEDOT:PSS thin film electrode with improved optics and electrochemical properties for transparent and flexible supercapacitor applications," *New J. Chem.*, vol. 46, no. 46, pp. 22130–22142, Nov. 2022, doi: 10.1039/D2NJ04194D.

[14] S. H. Choi *et al.*, "Diamond-like carbon as a buffer layer in polymeric electroluminescent device," *Thin Solid Films*, vol. 483, no. 1–2, pp. 351–357, Jul. 2005, doi: 10.1016/J.TSF.2004.12.040.

[15] S. Rafique, S. M. Abdullah, M. M. Shahid, M. O. Ansari, and K. Sulaiman, "Significantly improved photovoltaic performance in polymer bulk heterojunction solar cells with graphene oxide /PEDOT:PSS double decked hole transport layer," *Sci. Reports 2017 71*, vol. 7, no. 1, pp. 39555-, Jan. 2017, doi: 10.1038/srep39555.

[16] S. Shin, S. Cha, and G. Cho, "Fabrication of Electroconductive Textiles Based PLA Nanofiber Web Coatedwith PEDOT:4PSS," *Fash. Text. Res. J.*, vol. 22, no. 2, pp. 233–239, Apr. 2020, doi: 10.5805/SFTI.2020.22.2.233.

[17] C. Yin *et al.*, "A Novel and Facile One-Pot Solvothermal Synthesis of PEDOT-PSS/Ni-Mn-Co-O Hybrid as an Advanced Supercapacitor Electrode Material," *ACS Appl. Mater. Interfaces*, vol. 8, no. 4, pp. 2741–2752, Feb. 2016, doi: 10.1021/ACSAMI.5B11022.

[18] D. P. Mali, R. T. Patil, A. S. Patil, and V. J. Fulari, "Facile synthesis of NiO nanoflakes via hydrothermal route: Effect of urea concentration," *Chem. Phys. Lett.*, vol. 770, p. 138431, May 2021, doi: 10.1016/J.CPLETT.2021.138431.

[19] M. Imran, R. Ahmad, N. Afzal, and M. Rafique, "Copper ion implantation effects in ZnO film deposited on flexible polymer by DC magnetron sputtering," *Vacuum*, vol. 165, pp. 72–80, Jul. 2019, doi: 10.1016/J.VACUUM.2019.04.010.

[20] H. Xia, Y. Xiahou, P. Zhang, W. Ding, and D. Wang, "Revitalizing the Frens Method To Synthesize Uniform,Quasi-Spherical Gold Nanoparticles with Deliberately Regulated Sizesfrom 2 to 330 nm," *Langmuir*, vol. 32, no. 23, pp. 5870–5880, Jun. 2016, doi: 10.1021/ACS.LANGMUIR.6B01312.

[21] A. M. M. Hasan and M. A. B. H. Susan, "PEDOT:PSS polymer functionalized carbon nanotubes integrated with graphene oxide and titanium dioxide counter electrode for dye-sensitized solar cells," *Heliyon*, vol. 11, no. 3, p. e42272, Feb. 2025, doi: 10.1016/J.HELIYON.2025.E42272.

[22] H. T. Rahal, R. Awad, A. M. Abdel-Gaber, and D. E. S. Bakeer, "Synthesis,

Characterization, and Magnetic Properties of Pure and EDTA-Capped NiO Nanosized Particles," *J. Nanomater.*, vol. 2017, 2017, doi: 10.1155/2017/7460323.

[23] P. Dubey, Netram Kaurav, Rupesh S. Devan, G. S. Okram, and Y. K. Kuo, "The effect of stoichiometry on the structural, thermal and electronic properties of thermally decomposed nickel oxide," *RSC Adv.*, vol. 8, pp. 5882–5890, 2018, [Online]. Available: https://pdfs.semanticscholar.org/f4ee/c02aed37173c3c53fd0426e590086fbb585d.pdf

[24] P. Sakunpongpitiporn, K. Phasuksom, N. Paradee, and A. Sirivat, "Facile synthesis of highly conductive PEDOT:PSS via surfactant templates," *RSC Adv.*, vol. 9, no. 11, pp. 6363–6378, Feb. 2019, doi: 10.1039/C8RA08801B.

[25] C. Yeon, G. Kim, J. W. Lim, and S. J. Yun, "Highly conductive PEDOT:PSS treated by sodium dodecyl sulfate for stretchable fabric heaters," *RSC Adv.*, vol. 7, no. 10, pp. 5888–5897, Jan. 2017, doi: 10.1039/C6RA24749K.

[26] H. Machrafi, F. Iermano, S. Temsamani, I. Bobinac, and C. S. Iorio, "Enhanced electrical conductivity and stretchability of ionic-liquid PEDOT:PSS air-cathodes for aluminium-air batteries with long lifetime and high specific energy," *Sci. Reports 2022 121*, vol. 12, no. 1, pp. 22107-, Dec. 2022, doi: 10.1038/s41598-022-26546-8.

[27] B. H. Shetty *et al.*, "Fabrication of High-Performance MgCoO2/PEDOT:PSS@Nickel Foam Anode for Bioelectricity Generation by Microbial Fuel Cells," *J. Nanomater.*, vol. 2022, no. 1, p. 6358852, Jan. 2022, doi: 10.1155/2022/6358852.

[28] X. Xu, J. Gao, and W. Hong, "Ni-based chromite spinel for high-performance supercapacitors," *RSC Adv.*, vol. 6, no. 35, pp. 29646–29653, 2016, doi: 10.1039/C5RA27931C.

[29] F. I. Dar, K. R. Moonooswamy, and M. Es-Souni, "Morphology and property control of NiO nanostructures for supercapacitor applications," *Nanoscale Res. Lett. 2013 81*, vol. 8, no. 1, pp. 363-, Aug. 2013, doi: 10.1186/1556-276X-8-363.

[30] D. Jiang *et al.*, "NiO/NixCo3−xO4 porous ultrathin nanosheet/nanowire composite structures as high-performance supercapacitor electrodes," *RSC Adv.*, vol. 8, no. 56, p. 31853, 2018, doi: 10.1039/C8RA04827D.

[31] G. Greco *et al.*, "Pedot:PSS/Graphene Oxide (GO) Ternary Nanocomposites for Electrochemical Applications," *Molecules*, vol. 28, no. 7, p. 2963, Apr. 2023, doi: 10.3390/MOLECULES28072963/S1.

[32] G. Greco *et al.*, "Eco-Friendly EOG/PEDOT:PSS-Based Nanocomposites Blendedwith Green Additives for Flexible Supercapacitor Application," *ACS Appl. Eng. Mater.*, vol. 4, no. 2, pp. 1163–1176, Feb. 2026, doi: 10.1021/ACSAENM.5C01224.

[33] B. Tzaneva, M. Aleksandrova, V. Mateev, B. Stefanov, and I. Iliev, "Electrochemical Properties of PEDOT:PSS/Graphene Conductive Layers in Artificial Sweat," *Sensors 2024, Vol. 24, Page 39*, vol. 24, no. 1, p. 39, Dec. 2023, doi: 10.3390/S24010039.

[34] Y. Ge, X. Xie, J. Roscher, R. Holze, and Q. Qu, "How to measure and report the capacity of electrochemical double layers, supercapacitors, and their electrode materials," *J. Solid State Electrochem. 2020 2411*, vol. 24, no. 11, pp. 3215–3230, Aug. 2020, doi: 10.1007/S10008-020-04804-X.

[35] J. Liu *et al.*, "Advanced Energy Storage Devices: Basic Principles, Analytical Methods, and Rational Materials Design," *Adv. Sci.*, vol. 5, no. 1, p. 1700322, Jan. 2018, doi: 10.1002/ADVS.201700322;WGROUP:STRING:PUBLICATION.

[36] C. Yin *et al.*, "A Novel and Facile One-Pot Solvothermal Synthesis of PEDOT-PSS/Ni-Mn-Co-O Hybrid as an Advanced Supercapacitor Electrode Material," *ACS*

Appl. Mater. Interfaces, vol. 8, no. 4, pp. 2741–2752, Feb. 2016, doi: 10.1021/ACSAMI.5B11022.

[37] Y. M. Volfkovich, "Electrochemical Supercapacitors (a Review)," *Russ. J. Electrochem. 2021 574*, vol. 57, no. 4, pp. 311–347, May 2021, doi: 10.1134/S1023193521040108.

[38] J. Wang, J. Polleux, J. Lim, and B. Dunn, "Pseudocapacitive contributions to electrochemical energy storage in TiO 2 (anatase) nanoparticles," *J. Phys. Chem. C*, vol. 111, no. 40, pp. 14925–14931, Oct. 2007, doi: 10.1021/JP074464W.

[39] K. D. Fong, T. Wang, H. K. Kim, R. V. Kumar, and S. K. Smoukov, "Semi-Interpenetrating Polymer Networks for EnhancedSupercapacitor Electrodes," *ACS Energy Lett.*, vol. 2, no. 9, pp. 2014–2020, Sep. 2017, doi: 10.1021/ACSENERGYLETT.7B00466.

[40] B. Pal, S. Yang, S. Ramesh, V. Thangadurai, and R. Jose, "Electrolyte selection for supercapacitive devices: a critical review," *Nanoscale Adv.*, vol. 1, no. 10, pp. 3807–3835, Oct. 2019, doi: 10.1039/C9NA00374F.

[41] T. Kress, X. Liu, and A. C. Forse, "Pore network tortuosity controls fast charging in supercapacitors," *Nat. Mater. 2025 253*, vol. 25, no. 3, pp. 440–446, Nov. 2025, doi: 10.1038/s41563-025-02404-6.

[42] A. Lasia, "Electrochemical impedance spectroscopy and its applications," *Electrochem. Impedance Spectrosc. its Appl.*, vol. 9781461489337, pp. 1–367, Aug. 2014, doi: 10.1007/978-1-4614-8933-7/SAVE-RESEARCH.

[43] M. E. Orazem and B. Tribollet, "Electrochemical Impedance Spectroscopy," Apr. 2017, doi: 10.1002/9781119363682.

[44] H. Shi, C. Liu, Q. Jiang, and J. Xu, "Effective Approaches to Improve the Electrical Conductivity of PEDOT:PSS: A Review," *Adv. Electron. Mater.*, vol. 1, no. 4, Apr. 2015, doi: 10.1002/AELM.201500017.

[45] Q. Yang, S. K. Pang, and K. C. Yung, "Study of PEDOT–PSS in carbon nanotube/conducting polymer composites as supercapacitor electrodes in aqueous solution," *J. Electroanal. Chem.*, vol. 728, pp. 140–147, Aug. 2014, doi: 10.1016/J.JELECHEM.2014.06.033.

[46] Z. Li *et al.*, "Structural evolution of a Ni/NiOx based supercapacitor in cyclic charging-discharging: A polarized neutron and X-ray reflectometry study," *Electrochim. Acta*, vol. 290, pp. 118–127, Nov. 2018, doi: 10.1016/J.ELECTACTA.2018.09.051.

[47] Y. Li *et al.*, "A strong and highly flexible aramid nanofibers/PEDOT:PSS film for all-solid-state supercapacitors with superior cycling stability," *J. Mater. Chem. A*, vol. 4, no. 44, pp. 17324–17332, Nov. 2016, doi: 10.1039/C6TA06981A.

[48] X. hui Xia, J. ping Tu, X. li Wang, C. dong Gu, and X. bing Zhao, "Hierarchically porous NiO film grown by chemical bath deposition via a colloidal crystal template as an electrochemical pseudocapacitor material," *J. Mater. Chem.*, vol. 21, no. 3, pp. 671–679, 2011, doi: 10.1039/C0JM02784G.

[49] X. Yan, X. Tong, J. Wang, C. Gong, M. Zhang, and L. Liang, "Rational synthesis of hierarchically porous NiO hollow spheres and their supercapacitor application," *Mater. Lett.*, vol. 95, pp. 1–4, Mar. 2013, doi: 10.1016/J.MATLET.2012.12.073.

[50] B. Ren, M. Fan, Q. Liu, J. Wang, D. Song, and X. Bai, "Hollow NiO nanofibers modified by citric acid and the performances as supercapacitor electrode," *Electrochim. Acta*, vol. 92, pp. 197–204, Mar. 2013, doi: 10.1016/J.ELECTACTA.2013.01.009.

[51] J. Xu, L. Gao, J. Cao, W. Wang, and Z. Chen, "Electrochemical capacitance of nickel oxide nanotubes synthesized in anodic aluminum oxide templates," *J. Solid State Electrochem. 2010 159*, vol. 15, no. 9, pp. 2005–2011, Oct. 2010, doi: 10.1007/S10008-010-1222-6.

[52] Z. Zhou, H. Ni, and L. Z. Fan, "Hydrothermal synthesis of graphene/nickel oxide

nanocomposites used as the electrode for supercapacitors," *J. Nanosci. Nanotechnol.*, vol. 14, no. 7, pp. 4976–4981, 2014, doi: 10.1166/JNN.2014.8685.

[53] C. N. Chen, T. Ma, Q. Zhang, W. Fan, X. W. Fu, and Z. B. Wang, "Synthesis and Electrochemical Properties of Nitrogen-Doped Graphene (NG)/Nickle Oxide (NiO) Nanocomposite for Supercapacitor," *J. Nanosci. Nanotechnol.*, vol. 15, no. 12, pp. 9699–9704, Dec. 2015, doi: 10.1166/JNN.2015.11629.

[54] M. G. Fayed, D. Aman, and S. G. Mohamed, "Synergetic Electrochemical Behavior of NiO and Activated Carbon Composites for Advanced Supercapacitors," *J. Clust. Sci. 2025 363*, vol. 36, no. 3, pp. 94-, Apr. 2025, doi: 10.1007/S10876-025-02804-3.

[55] B. Wang *et al.*, "Mango Kernel-Derived Porous Carbon Confines Nano-NiO as an Efficient Bifunctional Electrode for Supercapacitors," *Bioresour.* , vol. 20, no. 4, pp. 11056–11065, 2025, doi: 10.15376/BIORES.20.4.11056-11065.

Supporting File:

```
"""
EIS equivalent-circuit fitting for two samples:
1. NiO-PEDOT:PSS
2. NiO
Circuit:
L - Rs - (Rct || CPE) - semi-infinite Warburg
Required input CSV files:
   EIS_NiO_PEDOT_PSS.csv
   EIS_NiO.csv
Each CSV must contain:
   frequency_Hz, Zreal_ohm, Zimag_ohm
The values supplied in the manuscript/table are used as initial estimates.
The optimizer refits the parameters from the experimental impedance data.
"""
import numpy as np
import pandas as pd
import matplotlib.pyplot as plt
from scipy.optimize import least_squares
from pathlib import Path
# ------------------------------------------------------------
# 1. SAMPLE SETTINGS AND REFERENCE INITIAL ESTIMATES
# ------------------------------------------------------------
# Inductance conversions:
# NiO-PEDOT:PSS: 931 x 10^-5 H = 9.31 x 10^-3 H
# NiO:           1431 x 10^-6 H = 1.431 x 10^-3 H
SAMPLES = {
   "NiO-PEDOT:PSS": {
      "file": "EIS_NiO_PEDOT_PSS.csv",
      "initial": [0.89, 5.44, 0.0977, 1.224, 73.997, 9.31e-3],
   },
   "NiO": {
      "file": "EIS_NiO.csv",
      "initial": [1.2181, 11.4800, 0.001738, 0.9559, 103.9903, 1.431e-3],
   },
}
# Bounds are deliberately broad. The upper bound for CPE-n is 1.5
# because the supplied NiO-PEDOT:PSS value is 1.224.
```

```
# Please verify this value and the circuit interpretation experimentally:
# CPE exponents above 1 are outside the usual 0 < n <= 1 range.
LOWER = np.array([0.0, 1e-8, 1e-12, 0.50, 0.0, 0.0], dtype=float)
UPPER = np.array([1e3, 1e6, 1e2, 1.50, 1e6, 1e-1], dtype=float)
OUTPUT_DIR = Path("EIS_fitting_results")
OUTPUT_DIR.mkdir(exist_ok=True)
# ------------------------------------------------------------
# 2. EQUIVALENT-CIRCUIT MODEL
# ------------------------------------------------------------
def impedance_model(params, omega):
    """
    params = [Rs, Rct, Q, n, sigma, L]
    Z = Rs + j*w*L + (Rct || CPE) + Zw
    """
    Rs, Rct, Q, n, sigma, L = params
    jw = 1j * omega
    z_cpe_parallel = 1.0 / (1.0 / Rct + Q * (jw ** n))
    z_warburg = sigma * (1.0 - 1j) / np.sqrt(omega)
    z_inductor = jw * L
    return Rs + z_inductor + z_cpe_parallel + z_warburg
# ------------------------------------------------------------
# 3. LOAD AND VALIDATE DATA
# ------------------------------------------------------------
def load_eis_data(filename):
    df = pd.read_csv(filename)
    required = ["frequency_Hz", "Zreal_ohm", "Zimag_ohm"]
    missing = [col for col in required if col not in df.columns]
    if missing:
        raise ValueError(
            f"{filename} is missing required column(s): {', '.join(missing)}"
        )
    f = df["frequency_Hz"].to_numpy(dtype=float)
    z_exp = (
        df["Zreal_ohm"].to_numpy(dtype=float)
        + 1j * df["Zimag_ohm"].to_numpy(dtype=float)
    )
    valid = (
        np.isfinite(f)
        & np.isfinite(z_exp.real)
        & np.isfinite(z_exp.imag)
        & (f > 0)
    )
    f, z_exp = f[valid], z_exp[valid]
    if len(f) < 7:
        raise ValueError(
            f"{filename} contains only {len(f)} valid points. "
            "At least 7 valid frequency points are required for this six-parameter fit."
        )
    order = np.argsort(f)
    f, z_exp = f[order], z_exp[order]
```

```
    omega = 2.0 * np.pi * f
    return f, omega, z_exp
# ------------------------------------------------------------
# 4. FIT ONE SAMPLE
# ------------------------------------------------------------
def fit_sample(sample_name, settings):
    filename = settings["file"]
    initial = np.asarray(settings["initial"], dtype=float)
    if not Path(filename).exists():
        raise FileNotFoundError(
            f"Input file not found: {filename}. "
            "Place the CSV file in the same folder as this script."
        )
    f, omega, z_exp = load_eis_data(filename)
    # Residual scaling: fit real and imaginary parts simultaneously.
    scale = np.maximum(np.abs(z_exp), 1.0)
    def residual(params):
        z_fit_local = impedance_model(params, omega)
        r = (z_fit_local - z_exp) / scale
        return np.r_[r.real, r.imag]
    fit = least_squares(
        residual,
        x0=initial,
        bounds=(LOWER, UPPER),
        max_nfev=100000,
        x_scale="jac",
    )
    params = fit.x
    Rs, Rct, Q, n, sigma, L = params
    z_fit = impedance_model(params, omega)
    # ------------------------------------------------------------
    # 5. FIT QUALITY
    # ------------------------------------------------------------
    err = z_fit - z_exp
    rmse_complex = np.sqrt(np.mean(np.abs(err) ** 2))
    norm_exp = np.linalg.norm(z_exp)
    relative_error_percent = (
        100.0 * np.linalg.norm(err) / norm_exp if norm_exp > 0 else np.nan
    )
    ss_res = np.sum(np.abs(z_exp - z_fit) ** 2)
    ss_tot = np.sum(np.abs(z_exp - np.mean(z_exp)) ** 2)
    r_squared_complex = (
        1.0 - ss_res / ss_tot if ss_tot > 0 else np.nan
    )
    # ------------------------------------------------------------
    # 6. PARAMETER AND FIT-QUALITY REPORT
    # ------------------------------------------------------------
    parameter_table = pd.DataFrame({
        "Sample": [sample_name] * 6,
        "Parameter": ["Rs", "Rct", "CPE-Q", "CPE-n", "Warburg sigma", "L"],
```

```
    "Fitted value": [Rs, Rct, Q, n, sigma, L],
    "Unit": [
        "ohm", "ohm", "S*s^n", "dimensionless",
        "ohm*s^(-1/2)", "H"
    ],
})
quality_table = pd.DataFrame([{
    "Sample": sample_name,
    "Complex RMSE (ohm)": rmse_complex,
    "Relative complex error (%)": relative_error_percent,
    "Complex R-squared diagnostic": r_squared_complex,
    "Optimizer success": fit.success,
    "Optimizer status": fit.status,
    "Optimizer message": fit.message,
    "Number of valid points": len(f),
}])
print(f"\n{'=' * 65}")
print(f"FITTED EQUIVALENT-CIRCUIT PARAMETERS: {sample_name}")
print(parameter_table[["Parameter", "Fitted value", "Unit"]].to_string(index=False))
print(f"\nComplex RMSE: {rmse_complex:.6g} ohm")
print(f"Relative complex error: {relative_error_percent:.3f} %")
print(f"Complex R-squared diagnostic: {r_squared_complex:.6f}")
print(f"Optimizer success: {fit.success}")
print(f"Optimizer message: {fit.message}")
# Save sample-specific parameter and fit-quality reports.
safe_name = (
    sample_name.replace(":", "")
    .replace("+", "_")
    .replace("-", "_")
    .replace(" ", "_")
)
parameter_table.to_csv(
    OUTPUT_DIR / f"{safe_name}_fitted_parameters.csv", index=False
)
quality_table.to_csv(
    OUTPUT_DIR / f"{safe_name}_fit_quality.csv", index=False
)
# Save experimental/fitted impedance and residuals.
output = pd.DataFrame({
    "frequency_Hz": f,
    "Zreal_exp_ohm": z_exp.real,
    "Zimag_exp_ohm": z_exp.imag,
    "Zreal_fit_ohm": z_fit.real,
    "Zimag_fit_ohm": z_fit.imag,
    "residual_real_ohm": err.real,
    "residual_imag_ohm": err.imag,
    "residual_magnitude_ohm": np.abs(err),
})
output.to_csv(OUTPUT_DIR / f"{safe_name}_fit_data.csv", index=False)
# ----------------------------------------------------------
```

```
    # 7. NYQUIST PLOT
    # ------------------------------------------------------------
    plt.figure(figsize=(7, 5))
    plt.plot(z_exp.real, -z_exp.imag, "o", ms=4, label="Experimental")
    plt.plot(z_fit.real, -z_fit.imag, "-", lw=2, label="Fitted model")
    plt.xlabel("Z' (ohm)")
    plt.ylabel("-Z" (ohm)")
    plt.title(f"Nyquist plot: {sample_name}")
    plt.grid(True, alpha=0.3)
    plt.legend()
    plt.tight_layout()
    plt.savefig(OUTPUT_DIR / f"{safe_name}_Nyquist_fit.png", dpi=300)
    plt.close()
    # ------------------------------------------------------------
    # 8. BODE MAGNITUDE AND PHASE PLOTS
    # ------------------------------------------------------------
    idx = np.argsort(f)
    f_plot = f[idx]
    z_exp_plot = z_exp[idx]
    z_fit_plot = z_fit[idx]
    plt.figure(figsize=(7, 5))
    plt.loglog(f_plot, np.abs(z_exp_plot), "o", ms=4, label="Experimental")
    plt.loglog(f_plot, np.abs(z_fit_plot), "-", lw=2, label="Fitted model")
    plt.xlabel("Frequency (Hz)")
    plt.ylabel("|Z| (ohm)")
    plt.title(f"Bode magnitude plot: {sample_name}")
    plt.grid(True, which="both", alpha=0.3)
    plt.legend()
    plt.tight_layout()
    plt.savefig(OUTPUT_DIR / f"{safe_name}_Bode_magnitude_fit.png", dpi=300)
    plt.close()
    phase_exp = np.angle(z_exp_plot, deg=True)
    phase_fit = np.angle(z_fit_plot, deg=True)
    plt.figure(figsize=(7, 5))
    plt.semilogx(f_plot, phase_exp, "o", ms=4, label="Experimental")
    plt.semilogx(f_plot, phase_fit, "-", lw=2, label="Fitted model")
    plt.xlabel("Frequency (Hz)")
    plt.ylabel("Phase angle (degree)")
    plt.title(f"Bode phase plot: {sample_name}")
    plt.grid(True, which="both", alpha=0.3)
    plt.legend()
    plt.tight_layout()
    plt.savefig(OUTPUT_DIR / f"{safe_name}_Bode_phase_fit.png", dpi=300)
    plt.close()
    return parameter_table, quality_table
# ------------------------------------------------------------
# 9. FIT BOTH SAMPLES AND SAVE COMBINED TABLES
# ------------------------------------------------------------
all_parameters = []
all_quality = []
```

```
for sample_name, settings in SAMPLES.items():
    parameter_table, quality_table = fit_sample(sample_name, settings)
    all_parameters.append(parameter_table)
    all_quality.append(quality_table)
combined_parameters = pd.concat(all_parameters, ignore_index=True)
combined_quality = pd.concat(all_quality, ignore_index=True)
combined_parameters.to_csv(
    OUTPUT_DIR / "EIS_comparison_fitted_parameters.csv", index=False
)
combined_quality.to_csv(
    OUTPUT_DIR / "EIS_comparison_fit_quality.csv", index=False
)
print("\nCOMBINED FITTED PARAMETERS")
print(combined_parameters.to_string(index=False))
print("\nCOMBINED FIT QUALITY")
print(combined_quality.to_string(index=False))
print(f"\nAll outputs saved in: {OUTPUT_DIR.resolve()}")
```



Copyright © by authors and 50Sea. This work is licensed under Creative Commons Attribution 4.0 International License.